



HAL
open science

Push–Pull Derivatives Based on 2,4'-Biphenylene Linker with Quinoxaline, [1,2,5]Oxadiazolo[3,4-B]Pyrazine and [1,2,5]Thiadiazolo[3,4-B]Pyrazine Electron Withdrawing Parts

Egor Verbitskiy, Pascal Le Poul, Filip Bureš, Sylvain Achelle, Alberto Barsella, Yuriy Kvashnin, Gennady Rusinov, Valery Charushin

► To cite this version:

Egor Verbitskiy, Pascal Le Poul, Filip Bureš, Sylvain Achelle, Alberto Barsella, et al.. Push–Pull Derivatives Based on 2,4'-Biphenylene Linker with Quinoxaline, [1,2,5]Oxadiazolo[3,4-B]Pyrazine and [1,2,5]Thiadiazolo[3,4-B]Pyrazine Electron Withdrawing Parts. *Molecules*, 2022, 27 (13), pp.4250. 10.3390/molecules27134250 . hal-03766446

HAL Id: hal-03766446

<https://hal.science/hal-03766446>

Submitted on 1 Sep 2022

HAL is a multi-disciplinary open access archive for the deposit and dissemination of scientific research documents, whether they are published or not. The documents may come from teaching and research institutions in France or abroad, or from public or private research centers.

L'archive ouverte pluridisciplinaire **HAL**, est destinée au dépôt et à la diffusion de documents scientifiques de niveau recherche, publiés ou non, émanant des établissements d'enseignement et de recherche français ou étrangers, des laboratoires publics ou privés.

Article

Push–Pull Derivatives Based on 2,4'-Biphenylene Linker with Quinoxaline, [1,2,5]Oxadiazolo[3,4-*B*]Pyrazine and [1,2,5]Thiadiazolo[3,4-*B*]Pyrazine Electron Withdrawing Parts

Egor V. Verbitskiy ^{1,2,*}, Pascal le Poul ³, Filip Bureš ^{4,*}, Sylvain Achelle ^{3,*}, Alberto Barsella ⁵, Yuriy A. Kvashnin ¹, Gennady L. Rusinov ^{1,2} and Valery N. Charushin ^{1,2}

¹ I. Postovsky Institute of Organic Synthesis, Ural Branch of the Russian Academy of Sciences, S. Kovalevskaya Str., 22, 620108 Ekaterinburg, Russia; kvashnin@ios.uran.ru (Y.A.K.); rusinov@ios.uran.ru (G.L.R.); valery-charushin-562@yandex.ru (V.N.C.)

² Department of Organic and Biomolecular Chemistry, Chemical Engineering Institute, Ural Federal University, Mira St. 19, 620002 Ekaterinburg, Russia

³ University Rennes, CNRS, Institut des Sciences Chimiques de Rennes—UMR 6226, 35000 Rennes, France; pascal.le-poul@univ-rennes1.fr

⁴ Institute of Organic Chemistry and Technology, Faculty of Chemical Technology, University of Pardubice Studenská 573, 53210 Pardubice, Czech Republic

⁵ Département d'Optique Ultrarapide et Nanophotonique, IPCMS, UMR CNRS 7504, Université de Strasbourg, 23 rue du Loess, BP 43, CEDEX 2, 67034 Strasbourg, France; alberto.barsella@ipcms.unistra.fr

* Correspondence: verbitskiye@yandex.ru (E.V.V.); filip.bures@upce.cz (F.B.); sylvain.achelle@univ-rennes1.fr (S.A.)



Citation: Verbitskiy, E.V.; le Poul, P.; Bureš, F.; Achelle, S.; Barsella, A.; Kvashnin, Y.A.; Rusinov, G.L.; Charushin, V.N. Push–Pull Derivatives Based on 2,4'-Biphenylene Linker with Quinoxaline, [1,2,5]Oxadiazolo[3,4-*B*]Pyrazine and [1,2,5]Thiadiazolo[3,4-*B*]Pyrazine Electron Withdrawing Parts. *Molecules* **2022**, *27*, 4250. <https://doi.org/10.3390/molecules27134250>

Academic Editor: Fernando Baiao Dias

Received: 11 June 2022

Accepted: 29 June 2022

Published: 30 June 2022

Publisher's Note: MDPI stays neutral with regard to jurisdictional claims in published maps and institutional affiliations.



Copyright: © 2022 by the authors. Licensee MDPI, Basel, Switzerland. This article is an open access article distributed under the terms and conditions of the Creative Commons Attribution (CC BY) license (<https://creativecommons.org/licenses/by/4.0/>).

Abstract: A series of novel V-shaped quinoxaline, [1,2,5]oxadiazolo[3,4-*b*]pyrazine and [1,2,5]thiadiazolo[3,4-*b*]pyrazine push–pull derivatives with 2,4'-biphenylene linker were designed and their electrochemical, photophysical and nonlinear optical properties were investigated. [1,2,5]Oxadiazolo[3,4-*b*]pyrazine is the stronger electron-withdrawing fragment as shown by electrochemical, and photophysical data. All compounds are emissive in a solid-state (from the cyan to red region of the spectrum) and quinoxaline derivatives are emissions in DCM solution. It has been found that quinoxaline derivatives demonstrate important solvatochromism and extra-large Stokes shifts, characteristic of twisted intramolecular charge transfer excited state as well as aggregation induced emission. The experimental conclusions have been justified by theoretical (TD-)DFT calculations.

Keywords: furazanopyrazine; [1,2,5]thiadiazolo[3,4-*b*]pyrazine; quinoxaline; donor–acceptor systems; twisted intramolecular charge transfer

1. Introduction

Push–pull derivatives with a D- π -A structure, where A and D are electron-withdrawing and electron-donating groups and the π represents a π -conjugated system, have been subject to a huge interest in the last decades due to their exceptional linear and nonlinear optical properties [1,2]. The D-A interaction into push–pull structures, also called intramolecular charge transfer (ICT), leads to the formation of low energy molecular orbitals whose electrons can be excited by visible light inducing colored materials [3–6]. The charge transfer absorption band will be red-shifted with an increase in the ICT strength. The limiting resonance forms of nitroaniline, a typical push–pull structure, are represented in Figure 1.

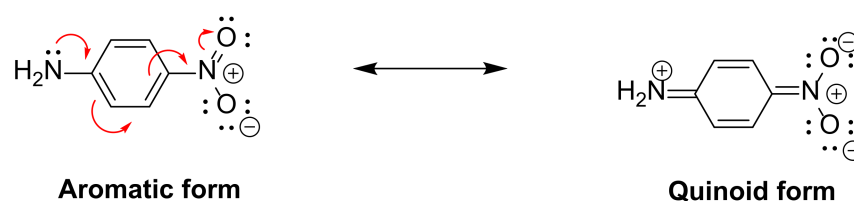


Figure 1. Limiting resonance forms of *p*-nitroaniline, a typical push–pull structure.

Push–pull molecular materials have found applications as fluorescent sensors [7–10], dye-sensitized solar cells (DSSC) [11–14], nonfullerene organic photovoltaic (OPV) materials [15–17], and numerous other optoelectronic devices [18–21]. The intramolecular charge transfer (ICT) in push–pull molecular materials can be modulated either by playing on the A/D couple [1,2,22,23] or by changing the nature and length of the π -conjugated bridge [1,2,24,25]. In this context, π -deficient heterocycles are particularly interesting as A part, as follows: the electron-lone pairs of heteroatoms of the heterocyclic core can be indeed used for protonation, complexation, alkylation, or the formation of a hydrogen bond, modifying their electron-withdrawing character and tuning the optical properties of corresponding push–pull structures by redistribution of charge density [26–31].

1,2,5-Chalcogenadiazoles and their annulated derivatives have received great attention due to the remarkable combination of their interesting properties, synthesis, and applications in materials sciences [32–35]. Recently, some of us designed and demonstrated the possible applications of [1,2,5]oxadiazolo[3,4-*b*]pyrazine derivatives (also called furazanopyrazines) as effective multifunctional chemosensors (I) [36,37], charge-transport materials for photovoltaics (II) [38], and compounds with advanced nonlinear optical (NLO) properties (III) (Figure 2) [39].

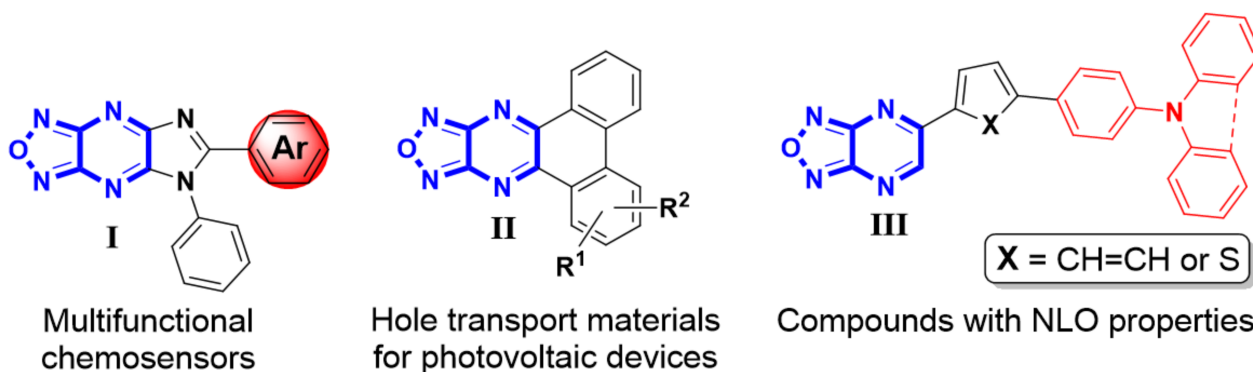


Figure 2. Representative compounds bearing furazanopyrazine scaffold.

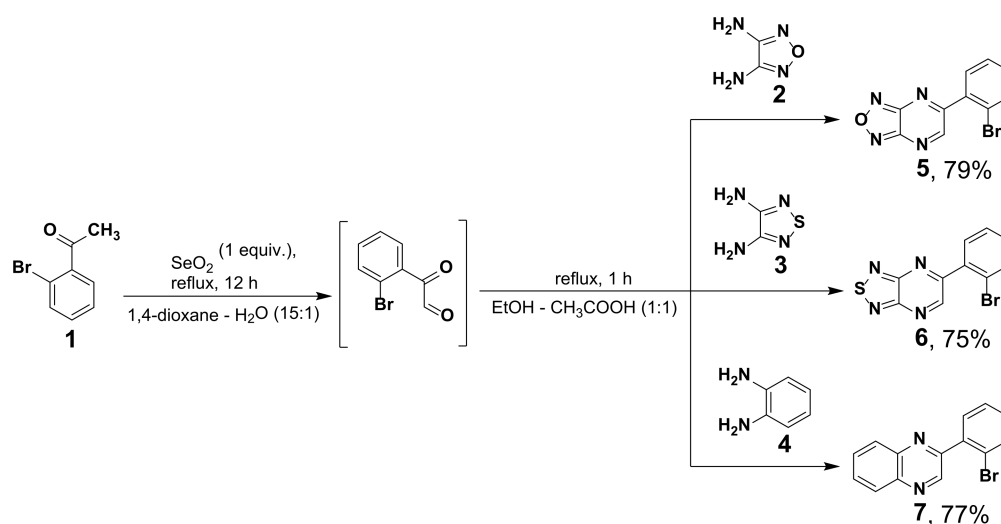
Phenylene bridges are typical linkers in push–pull structures, even if the aromaticity of the π -linker is directed toward the ICT [40,41]. The 1,4-phenylene unit is generally used, but the *ortho* arrangement can be interesting due to the steric hindrance that can lead to a twisted intramolecular charge transfer (TICT) excited state with large Stokes shifts [42,43].

This article is a further extension of our recent studies that are focused on the design of novel chromophores based on strong electron-withdrawing [1,2,5]oxadiazolo[3,4-*b*]pyrazine fragments [39]. Herein we report the synthesis of a new series of V-shaped D– π –A push–pull systems based on [1,2,5]oxadiazolo[3,4-*b*]pyrazine, [1,2,5]thiadiazolo[3,4-*b*]pyrazine, and quinoxaline acceptor cores and 2,4'-biphenylene π -linker. The systematic experimental investigation of their electronic and photophysical properties has been carried out, and these results were rationalized with the help of theoretical (TD)-DFT calculation.

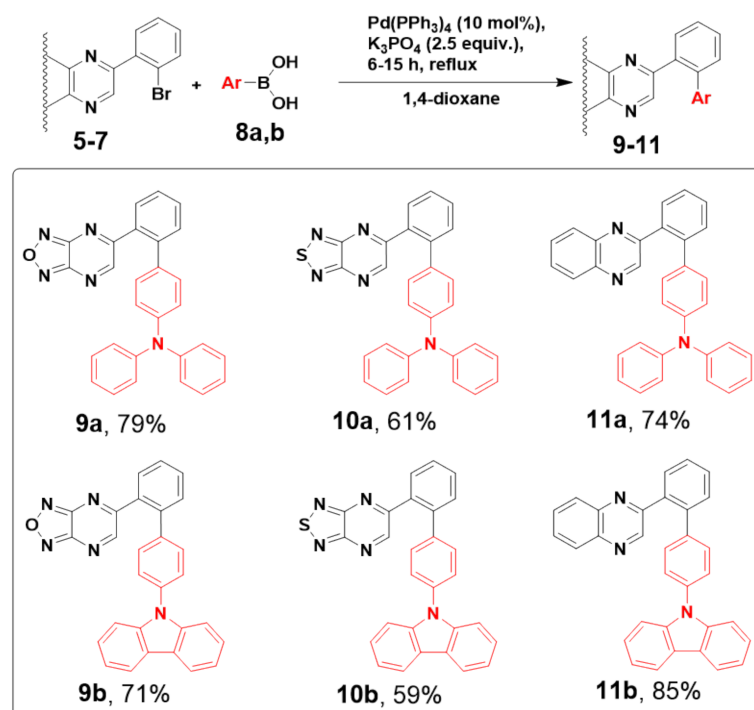
2. Results and Discussion

2.1. Synthesis

The target V-shaped push–pull 5-(4'-(*N,N*-diphenylamino)-[1,1'-biphenyl]-2-yl)-[1,2,5]oxadiazolo[3,4-*b*]pyrazine (**9a**) and 5-(4'-(9*H*-carbazol-9-yl)-[1,1'-biphenyl]-2-yl)-[1,2,5]oxadiazolo[3,4-*b*]pyrazine (**9b**) were prepared through two-step procedure according an early developed synthetic approach starting from commercially available 2'-bromoacetophenone (**1**) (Schemes 1 and 2) [39].



Scheme 1. Synthesis of 5-(2-bromophenyl)-[1,2,5]oxadiazolo[3,4-*b*]pyrazine (**5**), 5-(2-bromophenyl)-[1,2,5]thiadiazolo[3,4-*b*]pyrazine (**6**), and 2-(2-bromophenyl)quinoxaline (**7**).



Scheme 2. Synthesis and structure of V-shaped push–pull chromophores **9–11**.

In order to study the effect of the electron-withdrawing part on photophysical and electrochemical properties of the push–pull system, [1,2,5]thiadiazolo[3,4-*b*]pyrazine (**10a,b**) and quinoxaline (**11a,b**) structural analogues were synthesized. In this case, 1,2,5-thiadiazole-3,4-diamine (**3**) and *o*-phenylenediamine (**4**) were initially used to obtain corresponding

5-(2-bromophenyl)-[1,2,5]thiadiazolo[3,4-*b*]pyrazine (**6**) or 2-(2-bromophenyl)quinoxaline (**7**) with high yields (Scheme 1). All compounds were characterized by $^1\text{H}/^{13}\text{C}$ NMR and IR spectra as well as elemental analyses, and the results confirmed their structure.

In the second step, the desired chromophores **10a,b** and **11a,b** were obtained in good yields through the Suzuki–Miyaura cross-coupling reactions with the appropriate boronic acids **8a,b**, as shown in Scheme 2.

2.2. Electrochemical Properties

Electrochemical behavior of compounds **9–11** were studied by cyclic voltammetry in dichloromethane (DCM) containing Bu_4NPF_6 electrolyte at a scan rate of 0.1 V/s. The working electrode was a glassy carbon disk. A Pt wire was used as the counter electrode, and an Ag wire as a reference electrode. Ferrocene was used as an internal reference for potential measurements. The first oxidation/reduction peak potentials and their differences are listed in Table 1. Representative CV diagrams of compounds are shown in Figure 3.

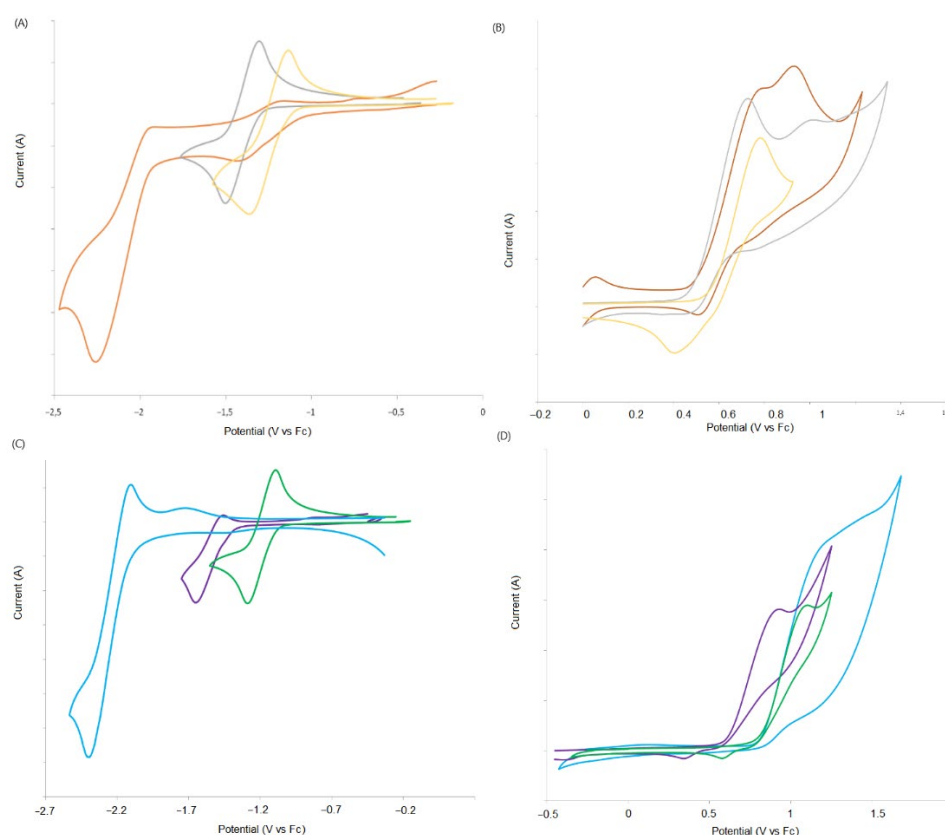


Figure 3. Cyclic voltammograms in DCM of compounds **9a** (yellow), **10a** (grey), and **11a** (red) in negative (A) and positive (B) direction and of **9b** (green), **10b** (purple), and **11b** (blue) in negative (C) and positive (D) direction.

Table 1. Electrochemical data of compounds **9–11**.

Compounds	E_{pa} [V] ^a	$E_{1/2}^{red}$ [V] ^a	ΔE [V] ^b	E_{HOMO} [eV] ^c	E_{LUMO} [eV] ^c	λ_{max} [nm] ^d
9a	0.79	−1.24	2.04	−5.59	−3.56	608
9b	1.08	−1.20	2.28	−5.88	−3.60	544
10a	0.72	−1.50	2.22	−5.52	−3.30	569
10b	0.87	−1.55	2.42	−5.67	−3.25	513
11a	0.74	−2.44	3.17	−5.54	−2.36	391
11b	1.10	−2.36 ^e	3.46	−5.90	−2.44	359

^a All potentials are given versus Fc/Fc⁺. ^b $\Delta E = E_{pa} - E_{1/2}^{red}$. ^c $E_{HOMO/LUMO} = -(E^{ox1/red1} + 4.8)$. ^d Calculated λ_{max} values ($\lambda = 1241/\Delta E$). ^e Irreversible peaks E_p .

Compounds **9b**, **10b**, and **11b** bearing a 9*H*-carbazol-9-yl fragment as an electron-donating group exhibit a first irreversible oxidation process at, respectively, 1.08 V, 0.87 V, and 1.10 V vs. Fc/Fc⁺. The measured maximum current intensity is high in comparison with the values obtained for reduction processes, indicating a possible polymerization reaction on the electrode. As a consequence, an irreversible reduction broad peak is detected between −0.67 and −0.84 V on the reverse scan only after the oxidation of compounds (Figure S1). Upon initial scanning in the negative direction, a reversible reduction is observed at −0.95 and −1.10 V, respectively, for **9b** and **10b**, and an irreversible reduction is observed at $E_{pc} = -2.36$ V for **11b**. When a donor is a diphenylamino group (compounds **9a**, **10a**, and **11a**), the first irreversible oxidation is shifted towards lower potentials as compared to the respective carbazole analogues **9b**, **10b**, and **11b**. This confirms the superior electron-donating strength of the diphenylamino moiety. For these compounds, the first oxidation is followed by a second one at a higher potential (Figure S2). The modification of the donor has a very weak influence on the reduction of the diazine (see Table 1 and Figure 3). These trends indicate a weak ground-state interaction between the donor and acceptor.

When comparing the reduction process of the electron-withdrawing fragments, the reduction potential increase in the following order **11** < **10** < **9**, indicating that the [1,2,5] oxadiazolo[3,4-*b*]pyrazine electron-withdrawing fragment is the strongest one. As a result, compound **9a**, bearing the strongest electron-donating and electron-withdrawing parts, showed the lowest electronic gap (ΔE) and is expected to exhibit the most red-shifted absorption bands across the whole series. Compared to their 1,4-phenylene analogues previously described [39], compounds **9a** and **9b** exhibited a larger electronic gap (0.65 V and 0.48 V) due to more difficult both oxidation and reduction processes, which indicates a significantly lower ICT.

2.3. Photophysical Properties

The UV-Vis and photoluminescence (PL) spectra of compounds **9–11** were measured in DCM solution at room temperature and the data are reported in Table 2. The UV/Vis spectra are provided in Figure 4. Regarding the lowest energetic absorption band, as expected according to electrochemical studies, the diphenylamino derivatives exhibit red-shifted absorption compared to their carbazole analogues. Similarly, as far as the electron-withdrawing part is concerned, the absorption maxima increase in the following order: **11** < **10** < **9** in both the diphenylamino and carbazole series. Compounds **9** and **10** are not luminescent in DCM solution, whereas the quinoxaline derivatives **11a** and **11b** exhibited green and yellow emissions, respectively, with low quantum yield. The particularly large Stokes shifts (>12,000 cm^{−1} for **11b**) could indicate the presence of a TICT excited state.

Table 2. Photophysical data of compounds **9–11** in DCM solution and in KBr matrix.

Compounds	DCM Solution			KBr Matrix
	λ_{abs} [nm] (ϵ [mM ^{−1} cm ^{−1}])	λ_{em} [nm] (Φ^a)	Stoke Shift (cm ^{−1})	λ_{em} [nm]
9a	327 (23.0), 508 (3.3)	- ^a	- ^a	755
9b	324 (13.4), 422 (2.3)	- ^a	- ^a	636
10a	335 (23.2), 479 (3.1)	- ^a	- ^a	662
10b	340 (16.8), 411sh (3.2)	- ^a	- ^a	588
11a	311 (25.0), 374 (6.3)	512 (0.03)	7206	478
11b	326 (11.6), 340 (10.9)	584 (0.01)	12,288	464

^a 9,10-diphenylethynylanthracene in cyclohexane as a standard ($\Phi_F = 1.00$).

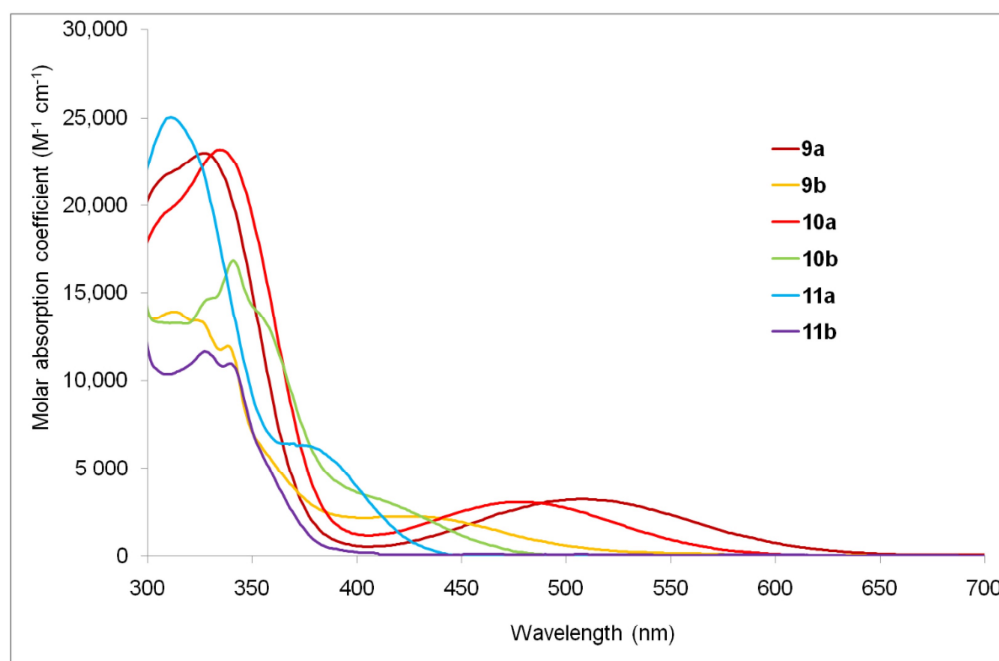


Figure 4. Absorption spectra of compounds 9–11 in DCM.

In an effort to gain further insight into the photophysical process within push–pull derivatives **11**, their emission spectra were registered in a series of aprotic solvents of increasing polarity. The positions of the corresponding emission maxima are reported in Table 3, and the normalized emission spectra registered for **11a**, as well as a picture of the solution in the various solvents, can be seen in Figures 5 and 6 (the same data are presented for compound **11b** in Figures S3 and S4). Whereas the position of the absorption maximum is not significantly affected by the polarity of the solvent, the position of the emission maxima is bathochromically shifted when the polarity of the solvent, which is estimated according to the Reichardt polarity scale [44], is increased. This pronounced positive emission solvatochromism is characteristic of ICT and is well documented for push–pull materials [45–48], in particular in the case of biphenylene linkers between **A** and **D** parts [49]. Large emission solvatochromism and low emission quantum yield in a polar solvent are characteristics of TICT [50,51].

Table 3. Emission solvatochromism of compounds **11**.

Compounds	λ_{em} [nm] ^a					
	<i>n</i> -Heptane $E_T(30) = 30.9$ ^a	Toluene $E_T(30) = 33.9$ ^a	1,4-Dioxane $E_T(30) = 36.0$ ^a	THF $E_T(30) = 37.4$ ^a	$CHCl_3$ $E_T(30) = 39.1$ ^a	DCM $E_T(30) = 40.7$ ^a
11a	456	487	521	534	573	584
11b	422	431	452	484	495	512

^a Reichardt polarity parameter ($kcal\ mol^{-1}$).

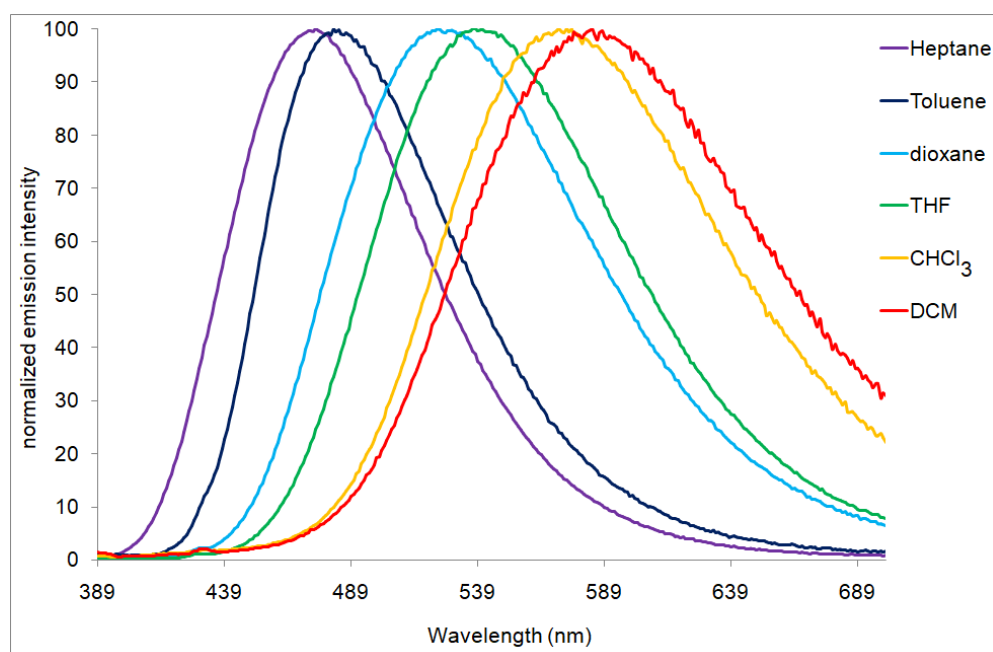


Figure 5. Normalized emission spectra of compound **11a** in a series of aprotic solvents ($c = 1 \times 10^{-5}$ M).



Figure 6. Fluorescence color change experienced by **11a** in various solvents (from left to right: *n*-heptane, toluene, 1,4-dioxane, CHCl_3 , DCM). The picture was taken in the dark upon irradiation with a handheld UV lamp ($\lambda_{\text{em}} = 366$ nm).

Aggregation-induced emission (AIE), a concept proposed by Tang and coworkers in 2001 [52,53], induces intensive emission in the solid-state of non- (or slightly) emissive chromophores in solution. A restriction of intramolecular motion is one of the mechanisms of AIE [53]. In order to study the potential AIE properties of compounds **11**, their emission spectra were recorded in a mixture of MeCN and water of a different ratio (Figure 7 and Figure S5). The pictures of the solutions under UV irradiation are presented in Figure 8 and Figure S6. For **11a**, no emission is observed in pure MeCN, while a dramatic increase in the emission intensity is observed when the water fraction is higher than 80%, inducing a new band centered at 519 nm. The highest intensity is observed for the water fraction of 97%. Compound **11b** is slightly emissive in pure MeCN with a yellow emission centered at 570 nm. When the ratio of water is increased, an extinction of the emission is initially observed (a water fraction of 50/60%), followed by the appearance of a new, blue-shifted

emission band ($\lambda_{\max} = 472$ nm) with the maximum intensity of 80% of water. For higher water fractions, the emission is slightly blue-shifted and lowered in intensity.

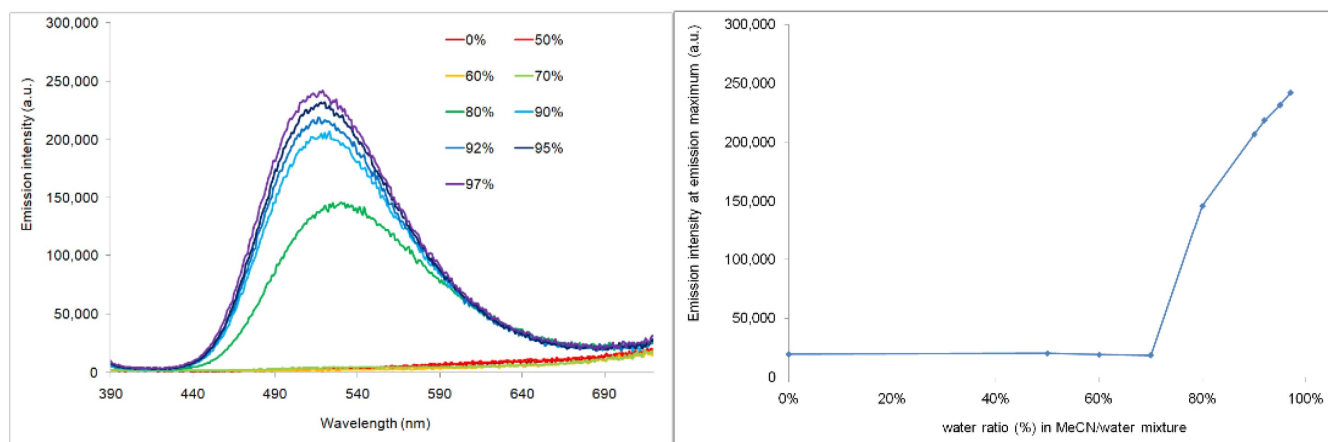


Figure 7. Left: Emission spectra of compound **11a** in MeCN/water mixture ($c = 1.5 \times 10^{-5}$ M, $\lambda_{\text{exc}} = 374$ nm), right: emission intensity of **11a** at emission maximum vs. water ratio in MeCN/water mixture.



Figure 8. Fluorescence color of compound **11a** in MeCN/water mixture (from left to right: 0% 50%, 80% 97% of water). The picture was taken in the dark upon irradiation with a handheld UV lamp ($\lambda_{\text{em}} = 366$ nm).

The compounds **9–11** are luminescent solids as measured in the KBr matrix. The emission maxima are listed in Table 2. The spectra and pictures of selected KBr pellets are presented in Figures 9 and 10. The KBr pellets exhibited intense emission from the blue for compound **11b** to near-infrared for compound **9a**. The emission is red-shifted in the same order as the emission bands recorded in solution.

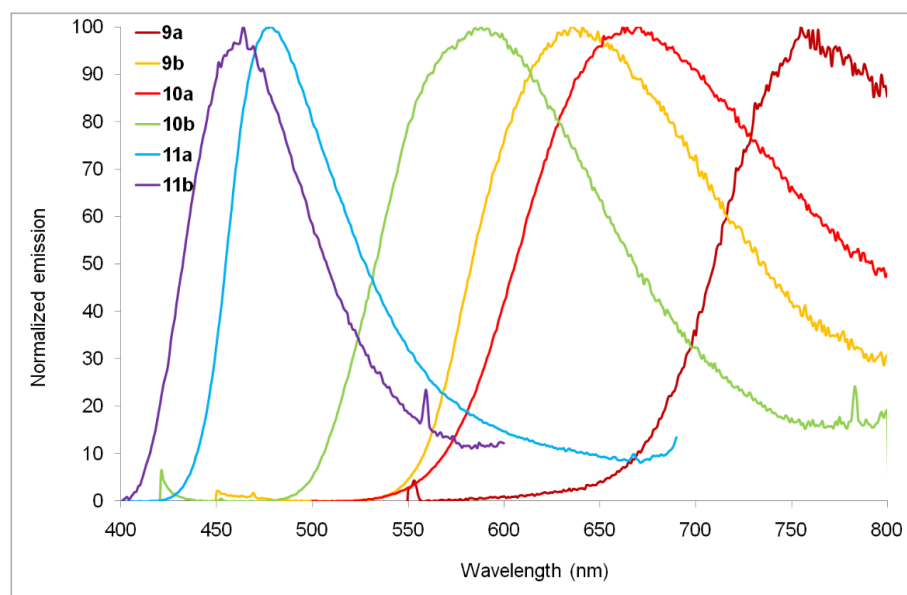


Figure 9. Normalized emission spectra of compounds **9–11** in KBr matrix (2 wt%).



Figure 10. Emission color of KBr pellets doped with 2% of chromophores (from left to right: **9b**, **10a**, **10b**, **11a**, **11b**). The picture was taken in the dark upon irradiation with a handheld UV lamp ($\lambda_{\text{exc}} = 366 \text{ nm}$).

2.4. NLO Properties

The second-order NLO properties of compounds **9–11** have been investigated in chloroform using the electric-field induced second harmonic generation (EFISH) method at a non-resonant incident wavelength of 1907 nm. The EFISH method provides an estimation of the NLO response as the scalar product between the permanent dipole moment of the molecule $\vec{\mu}$ and the vector component of β described as $\beta_{//}$ [54–56]. The data are reported in Table 4. The NLO responses of compounds **9–11** are particularly low and we are close to the limit of detection of the system. It is therefore not reasonable to compare the values between them. For the 1,4-phenylene analogue of compounds **9a**, a much higher $\mu\beta$ value was measured ($700 \times 10^{-48} \text{ esu}$) [39]. This indicates that the 1,2-phenylene arrangement drastically reduces the NLO response due to the limited/diminished ICT.

Table 4. Results of EFISH measurements for compounds **9–11**.

	9a	9b	10a	10b	11a	11b
$\mu\beta$ (10^{-48} esu)	80	20	80	50	40	0

2.5. Theoretical Calculation

Molecular structures and electronic properties of V-shaped push–pull chromophores **9–11** were theoretically investigated using the Gaussian 16 software package [57]. First, the geometries were optimized using the DFT B3LYP/6-311+G(2df,p) method in CHCl_3 . Using the same level of theory, the energies of the frontier molecular orbitals (HOMO/LUMO), ground-state dipole moments (μ), and first hyperpolarizabilities (β) were subsequently calculated. All the calculated data are gathered in Table 5; see the ESI for further information.

Table 5. DFT-calculated data of compounds 9–11.

Compounds	$E_{\text{HOMO}}^{\text{DFT}}$ [eV]	$E_{\text{LUMO}}^{\text{DFT}}$ [eV]	ΔE^{DFT} [eV]	μ [D]	$\lambda_{\text{max}}^{\text{TD-DFT}}$ [nm/eV]	$\beta(-2\omega, \omega, \omega)^{\text{DFT}}$ [10^{-30} esu]
9a	−5.49	−3.45	2.04	8.11	447/2.77	504
9b	−5.84	−3.55	2.29	7.86	377/3.29	117
10a	−5.43	−3.26	2.17	4.24	420/2.95	311
10b	−5.81	−3.34	2.47	4.30	357/3.47	74
11a	−5.36	−2.33	3.03	0.87	335/3.70	53
11b	−5.77	−2.40	3.37	2.37	301/4.12	18

All data calculated at the DFT level by using the Gaussian[®] 16 software package and DFT B3LYP/6-311+G(2df,p) method in CHCl_3 . The first hyperpolarizabilities $\beta(-2\omega, \omega, \omega)$ were calculated at 1907 nm. The electronic absorption spectra, the longest-wavelength absorption maxima and the corresponding electron transitions were calculated using TD-DFT ($n_{\text{states}} = 8$) B3LYP/6-311+G(2df,p).

The optimized geometries of 9–11 are shown in Figure 11A. As can be seen, the central biphenylene π -linker, interconnecting the *N,N*-diphenylamino, and pyrazine-derived moieties, adopts twisted geometry with the central torsion angle between 20° and 60° . Carbazole derivatives **b** showed generally larger torsion angles. The heterocyclic moiety at position 2 is always turned out by about 45° , independently of the particular derivative. The bond length alternation of both 1,4-phenylene moieties of the π -linker was investigated, revealing the Bird index I_6 and the quinoid character (δr) within the range of 91–96/2–5% [58,59]. For unsubstituted benzene, the I_6 and δr are equal to 100 and 0, respectively. The calculated values imply that both 1,4-phenylene moieties in 9–11 are slightly polarized. Alternation of the heterocyclic acceptor significantly affected the ground state dipole moment of V-shaped chromophores. The largest ones were calculated for furazanopyrazine derivatives **9**, while replacement of the fused terminal oxa/thiadiazolo fragment by benzene diminished the dipole moment significantly as seen for **11**.

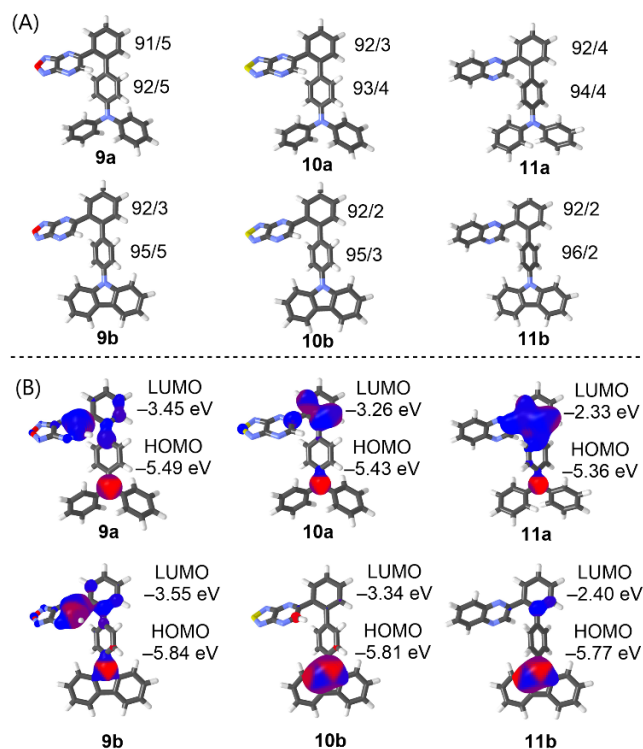


Figure 11. DFT-optimized geometries including Bird index/quinoid character of the particular 1,4-phenylene moieties (A) and HOMO (red) and LUMO (blue) localizations (B) in chromophores 9–11.

The calculated energies of the frontier molecular orbitals ($E_{\text{HOMO/LUMO}}$) and their differences E are summarized in Table 5. The latter quantity correlates tightly with the electrochemical gaps (Figure S7). The oxadiazolopyrazine acceptor moiety in **9a–b** im-

parts the strongest ICT with the lowest calculated HOMO–LUMO gaps as compared to chromophores **10** and **11**. When comparing the triads of chromophores **a** and **b**, *N,N*-diphenylamino-substituted derivatives **a** possess lower HOMO–LUMO gaps than the corresponding carbazole derivatives **b**. Figure 9B shows HOMO and LUMO localizations in the particular derivatives; an obvious charge-separation is seen for **9a** and **9b**. For *N,N*-diphenylamino-substituted derivatives **10a** and **11a** are the situation similar, which is in contrast to carbazoles **10b** and **11b**. In these derivatives, both HOMO and LUMO are predominantly cumulated over the carbazole's nitrogen atom, which results in their diminished ICT character and larger ΔE values.

Fundamental optical properties of **9–11** were investigated by TD-DFT CAM-B3LYP/6-311+G(2df,p) (nstates = 8) method. The calculated electronic absorption spectra along with the experimental ones are visualized in Figure S8. Both spectra feature the same shape and number of peaks and mostly differ in the position of the longest-wavelength absorption maxima. The λ_{\max} values listed in Table 5 showed a very tight correlation with the experimental ones (Table 1)—see Figure S9. According to the aforementioned discussion on the HOMO–LUMO gap, oxadiazolopyrazine chromophores **9a–b** possess the most bathochromically shifted absorption maxima. Hence, both O→S replacement and fusing of benzene rings as in **10** and **11** shift the absorption maxima hypsochromically. An inspection of the transition forming the particular bands revealed that the longest wavelength absorption bands of chromophores **9a–b**, **10a**, and **11a** are generated by the HOMO→LUMO transition and these can be designed as CT bands. The corresponding high-energy bands (blue shifted) involve also the HOMO–1→LUMO and the HOMO→LUMO+1 transitions. On the contrary, the absorption of chromophores **10b** and **11b** is dominated by the HOMO–2→LUMO transition, with a weak contribution of the HOMO→LUMO transition seen for **10b**. These observations agree with their largest HOMO–LUMO gaps and the most hypsochromically shifted spectra.

The first order hyperpolarizability $\beta(-2\omega, \omega, \omega)$ calculated at 1907 nm is listed in Table 5. As can be seen, the largest polarizabilities were calculated for chromophores **9a** and **10a**, similarly to the EFISH experiment. Oxadiazolopyrazine, or eventually thiadiazolopyrazine, in combination with an *N,N*-diphenylamino substituent, is the most useful electron acceptor/donor pair in V-shaped NLOphores **9–11**.

3. Experimental Methods

3.1. General Information

All reagents and solvents were obtained from commercial sources and dried by using standard procedures before use. Starting materials **5** and **7** were prepared according to the earlier reported procedure [60]. The ^1H and ^{13}C NMR spectra were recorded on a Bruker AVANCE-600 instruments using Me_4Si as an internal standard. Elemental analysis was carried on a Eurovector EA 3000 automated analyzer. Melting points were determined on Boetius combined heating stages and were not corrected. The chromatographic purification of compounds was achieved with silica gel Alfa Aesar 0.040–0.063 mm (230–400 mesh), eluting with CH_2Cl_2 /hexane (1:2, *v/v*). The progress of reactions and the purity of compounds were checked by TLC on Sorbfil plates (Russia), in which the spots were visualized with UV light (λ 254 or 365 nm). IR spectra of samples (solid powders) were recorded on a Spectrum One Fourier transform IR spectrometer (Perkin Elmer, Waltham, MA, USA) equipped with a diffuse reflectance attachment (DRA) in the frequency range $4000 \div 400 \text{ cm}^{-1}$. Spectrum processing and band intensity determination were carried out using the special software supplied with the spectrometer.

3.2. Electrochemical Characterization

The electrochemical studies of the compounds were performed with a home-designed 3-electrodes cell (WE: glassy carbon disk, RE: Ag wire, Ce: Pt). Ferrocene was added at the end of each experiment to determine redox potential values.

3.3. Photophysical Characterization

The absorption spectra of the samples were detected with a JASCO V-650 instrument, whereas the emission spectra were detected by a Horiba Fluoromax spectrophotometer. UV/Vis and fluorescence spectra were recorded by using standard 1 cm quartz cells. Compounds were excited at their absorption maxima in solution (band of lowest energy) to record the emission spectra. The Φ_F values were calculated by using a well-known procedure with 9,10-diphenylethynylanthracene in cyclohexane as a standard ($\Phi_F = 1.00$) [61]. Stokes shifts were calculated by considering the lowest energy absorption band. Experimental details on EFISH measurements are described elsewhere [62].

Synthesis of 5-(2-bromophenyl)-[1,2,5]thiadiazolo[3,4-*b*]pyrazine (6). A mixture of 2'-bromoacetophenone **1** (1.994 g, 10 mmol) and selenium dioxide (1.1 g, 10 mmol) in a solution of 1,4-dioxane (15 mL) and water (1 mL) was refluxed for 12 h. Selenium was filtered off and washed with 1,4-dioxane (5 mL). The solvent was evaporated at reduced pressure. The residue was dissolved in a mixture of ethanol (5 mL) and acetic acid (5 mL), 1,2,5-thiadiazole-3,4-diamine (**3**) (1.16 g, 10 mmol) was added, and the resulting mixture was refluxed for 1 h and cooled to room temperature. A precipitate formed was filtered, washed with ethanol, and dried in air. Compound **6** was obtained as a pale-yellow solid. Yield 2.2 g (75%), mp 169–170 °C. The ^1H NMR (600 MHz, DMSO- d_6) δ 9.45 (s, 1H), 7.90 (dd, $J = 8.1, 1.1$ Hz, 1H), 7.79 (dd, $J = 7.6, 1.7$ Hz, 1H), 7.66 (td, $J = 7.5, 1.1$ Hz, 1H), 7.57 (td, $J = 7.7, 1.7$ Hz, 1H). The ^{13}C NMR (151 MHz, DMSO- d_6) δ 158.2, 154.0, 153.4, 151.7, 137.3, 133.7, 132.8, 132.7, 128.9, 121.7. Calcd. For $\text{C}_{10}\text{H}_5\text{BrN}_4\text{S}$ (293.14): C, 40.97; H, 1.72; N, 19.11. Found: C, 41.02; H, 1.77; N, 19.16.

General procedure for the synthesis of 5-(4'-(heteroaryl)-[1,1'-biphenyl]-2-yl)-[1,2,5]oxadiazolo[3,4-*b*]pyrazine (9), 5-(4'-(heteroaryl)-[1,1'-biphenyl]-2-yl)-[1,2,5]thiadiazolo[3,4-*b*]pyrazine (10), and 2-(4'-(heteroaryl)-[1,1'-biphenyl]-2-yl)-quinoxaline (11). A mixture of 5-(2-bromophenyl)-[1,2,5]oxadiazolo[3,4-*b*]pyrazine (**5**) (277 mg, 1.0 mmol), 5-(2-bromophenyl)-[1,2,5]thiadiazolo[3,4-*b*]pyrazine (**6**) (293 mg, 1.0 mmol) or 2-(2-bromophenyl)quinoxaline (**7**) (285 mg, 1.0 mmol), corresponding arylboronic acid **8a** or **8b** (1.2 mmol), $\text{Pd}(\text{PPh}_3)_4$ (115 mg, 10 mol %) and K_3PO_3 (530 mg, 2.5 mmol) were dissolved in 1,4-dioxane (15 mL). The reaction mixture was degassed and refluxed for 15 h under an argon atmosphere. After completion of the reaction (as monitored by TLC), the reaction mixture was cooled, filtered, and dissolved in a mixture of EtOAc and water (1:1, 50 mL). The organic layer was separated, the aqueous layer was extracted with EtOAc (2 \times 25 mL), the combined organic extracts were dried with MgSO_4 and the solvents were evaporated. Purification by silica gel column chromatography with CH_2Cl_2 /hexane (1:2, *v/v*) as an eluent afforded the title compounds **9–11**.

2'-([1,2,5]Oxadiazolo[3,4-*b*]pyrazin-5-yl)-*N,N*-diphenyl-[1,1'-biphenyl]-4-amine (9a). Yield 348 mg (79%), dark violet solid, mp 160–161 °C. The ^1H NMR (600 MHz, DMSO- d_6) δ 8.31 (s, 1H), 7.91 (d, $J = 7.7$ Hz, 1H), 7.76 (t, $J = 7.5$ Hz, 1H), 7.69–7.63 (m, 2H), 7.32 (t, $J = 7.7$ Hz, 4H), 7.17 (d, $J = 8.2$ Hz, 2H), 7.10–7.04 (m, 6H), 6.91 (d, $J = 8.2$ Hz, 2H). The ^{13}C NMR (151 MHz, DMSO- d_6) δ 164.5, 157.3, 152.8, 151.3, 148.0, 147.1, 141.4, 134.4, 132.7, 132.5, 131.8, 131.6, 130.5, 130.1, 128.5, 125.1, 124.2, 122.8. Calcd. for $\text{C}_{28}\text{H}_{19}\text{N}_5\text{O}$ (441.49): C, 76.17; H, 4.34; N, 15.86. Found: C, 76.24; H, 4.46; N, 15.70. ν (DRA, cm^{-1}) 3061 (w, C-H_{Ar}), 3036 (w, C-H_{Ar}), 1588 (s, C-C_A/C-N_{Ar}), 1487 (s, C-C_{Ar}/C-N_{Ar}), 1443 (s, C-C_{Ar}/C-N_{Ar}), 753 (s, C-H_{Ar}), 695 (s, C-H_{Ar}).

5-(4'-(9*H*-Carbazol-9-yl)-[1,1'-biphenyl]-2-yl)-[1,2,5]oxadiazolo[3,4-*b*]pyrazine (9b). Yield 311 mg (71%), red-orange solid, mp 226–227 °C. The ^1H NMR (600 MHz, DMSO- d_6) δ 8.50 (s, 1H), 8.26 (dt, $J = 7.8, 0.9$ Hz, 2H), 8.00 (dd, $J = 7.7, 1.2$ Hz, 1H), 7.88–7.82 (m, 2H), 7.75 (ddd, $J = 7.7, 6.9, 1.8$ Hz, 1H), 7.65–7.62 (m, 2H), 7.60–7.56 (m, 2H), 7.46 (ddd, $J = 8.3, 7.1, 1.2$ Hz, 2H), 7.38 (dt, $J = 8.2, 0.9$ Hz, 2H), 7.31 (ddd, $J = 7.9, 7.1, 1.0$ Hz, 2H). The ^{13}C NMR (151 MHz, DMSO- d_6) δ 164.2, 157.3, 152.9, 151.4, 141.0, 140.4, 138.6, 137.3, 134.8, 132.7, 132.3, 132.1, 131.0, 129.2, 127.6, 126.8, 123.4, 121.1, 120.8, 110.0. Calcd. for $\text{C}_{28}\text{H}_{17}\text{N}_5\text{O}$ (439.48): C, 76.52; H, 3.90; N, 15.94. Found: C, 76.47; H, 3.78; N, 15.82. ν (DRA, cm^{-1}) 3060 (w, C-H_{Ar}), 1600 (s, C-C_{Ar}/C-N_{Ar}), 1450 (s, C-C_{Ar}/C-N_{Ar}), 749 (s, C-H_{Ar}), 724 (s, C-H_{Ar}).

2'-([1,2,5]Thiadiazolo[3,4-*b*]pyrazin-5-yl)-*N,N*-diphenyl-[1,1'-biphenyl]-4-amine (10a). Yield 278 mg (61%), bright orange solid, mp 189–190 °C. The ¹H NMR (600 MHz, DMSO-*d*₆) δ 8.48 (s, 1H), 7.89 (dd, *J* = 7.7, 1.3 Hz, 1H), 7.71 (td, *J* = 7.5, 1.4 Hz, 1H), 7.63 (ddd, *J* = 14.9, 7.6, 1.3 Hz, 2H), 7.34–7.29 (m, 4H), 7.13–7.09 (m, 2H), 7.08–7.04 (m, 2H), 7.04–7.00 (m, 4H), 6.89–6.85 (m, 2H). The ¹³C NMR (151 MHz, DMSO-*d*₆) δ 159.9, 154.5, 152.8, 152.1, 147.5, 147.2, 141.2, 135.1, 133.5, 131.7, 131.5, 131.5, 130.6, 130.1, 128.4, 124.9, 124.0, 123.0. Calcd. for C₂₈H₁₉N₅S (457.56): C, 73.50; H, 4.19; N, 15.31. Found: C, 73.23; H, 4.24; N, 15.21. ν (DRA, cm⁻¹) 3085 (w, C–H_{Ar}), 3064 (w, C–H_{Ar}), 3025 (w, C–H_{Ar}), 1594 (s, C–C_A/C–N_{Ar}), 1483 (s, C–C_{Ar}/C–N_{Ar}), 754 (s, C–H_{Ar}), 693 (s, C–H_{Ar}).

5-(4'-(9*H*-Carbazol-9-yl)-[1,1'-biphenyl]-2-yl)-[1,2,5]thiadiazolo[3,4-*b*]pyrazine (10b). Yield 268 mg (59%), yellow solid, mp 250–251 °C. The ¹H NMR (600 MHz, DMSO-*d*₆) δ 8.65 (s, 1H), 8.24 (d, *J* = 7.8 Hz, 2H), 7.98 (d, *J* = 7.6 Hz, 1H), 7.80 (q, *J* = 5.1, 4.2 Hz, 2H), 7.73 (td, *J* = 6.8, 5.7, 2.9 Hz, 1H), 7.61–7.48 (m, 4H), 7.44 (t, *J* = 7.6 Hz, 2H), 7.36–7.25 (m, 4H). The ¹³C NMR (151 MHz, DMSO-*d*₆) δ 159.5, 154.5, 152.9, 152.0, 140.8, 140.4, 139.2, 136.8, 135.4, 132.1, 132.0, 131.7, 131.0, 129.1, 127.4, 126.7, 123.3, 121.1, 120.7, 110.0. Calcd. for C₂₈H₁₇N₅S (455.54): C, 73.83; H, 3.76; N, 15.37. Found: C, 73.70; H, 3.75; N, 15.24. ν (DRA, cm⁻¹) 3060 (w, C–H_{Ar}), 3042 (w, C–H_{Ar}), 1597 (s, C–C_{Ar}/C–N_{Ar}), 1452 (s, C–C_{Ar}/C–N_{Ar}), 751 (s, C–H_{Ar}), 725 (s, C–H_{Ar}).

***N,N*-Diphenyl-2'-(quinoxalin-2-yl)-[1,1'-biphenyl]-4-amine (11a).** Yield 332 mg (74%), pale yellow solid, mp 135–137 °C. The ¹H NMR (600 MHz, DMSO-*d*₆) δ 8.41 (s, 1H), 8.07 (ddd, *J* = 8.5, 7.1, 1.6 Hz, 2H), 7.89–7.82 (m, 3H), 7.63 (td, *J* = 7.1, 6.6, 1.5 Hz, 1H), 7.60–7.55 (m, 2H), 7.30–7.23 (m, 4H), 7.02 (dd, *J* = 7.9, 5.9 Hz, 4H), 6.99–6.95 (m, 4H), 6.86–6.80 (m, 2H). The ¹³C NMR (151 MHz, DMSO-*d*₆) δ 154.9, 147.3, 147.0, 146.9, 142.1, 140.9, 140.4, 136.4, 134.6, 131.4, 131.2, 130.7, 130.5, 130.40, 130.38, 130.0, 129.5, 129.3, 128.3, 124.4, 123.7, 123.4. Calcd. for C₃₂H₂₃N₃ (449.56): C, 85.50; H, 5.16; N, 9.35. Found: C, 85.49; H, 5.36; N, 9.29. ν (DRA, cm⁻¹) 3057 (w, C–H_{Ar}), 3034 (w, C–H_{Ar}), 1585 (s, C–C_A/C–N_{Ar}), 1492 (s, C–C_{Ar}/C–N_{Ar}), 1481 (s, C–C_{Ar}/C–N_{Ar}), 752 (s, C–H_{Ar}), 694 (s, C–H_{Ar}).

9-(2'-(Quinoxalin-2-yl)-[1,1'-biphenyl]-4-yl)-9*H*-carbazole (11b). Yield 379 mg (85%), pale yellow solid, mp 158–159 °C. The ¹H NMR (600 MHz, DMSO-*d*₆) δ 8.56 (s, 1H), 8.25–8.21 (m, 2H), 8.08 (td, *J* = 8.5, 1.7 Hz, 2H), 7.93 (dd, *J* = 7.4, 1.1 Hz, 1H), 7.90–7.84 (m, 2H), 7.75–7.71 (m, 2H), 7.70–7.66 (m, 1H), 7.52–7.49 (m, 2H), 7.41 (dd, *J* = 8.9, 7.3 Hz, 4H), 7.31–7.26 (m, 4H). The ¹³C NMR (151 MHz, DMSO-*d*₆) δ 154.6, 146.9, 142.1, 140.6, 140.5, 140.5, 139.9, 136.7, 136.4, 131.8, 131.5, 130.9, 130.8, 130.6, 130.5, 129.6, 129.3, 128.9, 127.2, 126.7, 123.2, 121.0, 120.6, 109.9. Calcd. for C₃₂H₂₁N₃ (447.54): C, 85.88; H, 4.73; N, 9.39. Found: C, 85.95; H, 4.85; N, 9.41. ν (DRA, cm⁻¹) 3055 (w, C–H_{Ar}), 3042 (w, C–H_{Ar}), 1598 (s, C–C_{Ar}/C–N_{Ar}), 1450 (s, C–C_{Ar}/C–N_{Ar}), 748 (s, C–H_{Ar}), 724 (s, C–H_{Ar}).

4. Conclusions

In summary, we have designed a series of push–pull chromophores bearing quinoxaline, [1,2,5]oxadiazolo[3,4-*b*]pyrazine, and [1,2,5]thiadiazolo[3,4-*b*]pyrazine as A part and 2,4'-biphenylene as a π-conjugated linker. The [1,2,5]oxadiazolo[3,4-*b*]pyrazine fragment appears as the strongest A part according to experimental electrochemical and photophysical results and theoretical calculation. With regards to 4,4'-biphenylene and 1,4-phenylene-2,5-thienylene known analogues, these compounds exhibit reduced ICT leading to a low NLO response. Nevertheless, all compounds exhibited intense emissions in the solid state ranging from cyan to red/near-infrared. Quinoxaline derivatives **11** exhibited TICT emission with intense solvatochromism, large Stokes shifts, and AIE.

Supplementary Materials: The following supporting information can be downloaded at: <https://www.mdpi.com/article/10.3390/molecules27134250/s1>, Figures S1 and S2: Oxidation study of compounds **9b**, **10b**, **11a**, and **11b** Figure S3: Normalized emission spectra of compound **11b** in a series of aprotic solvents. Figure S4: Fluorescence color change experienced by **11b** in various solvents. Figure S5: Emission spectra of compound **11b** in MeCN/water mixture. Figure S6: Fluorescence color of compound **11b** in MeCN/water mixture. Figure S7: A correlation of the experimental (ELCH) and DFT-calculated HOMO–LUMO gaps of chromophores **9–11**. Figure S8: TD-DFT (nstates = 8)

B3LYP/6-311+G(2d,f,p) calculated UV-Vis spectra of chromophores 9–11 in CHCl₃ (red curves) along with the experimental spectra (black curves). Red vertical lines represent oscillator strengths (f). Figure S9: A correlation of the experimental (EXP) and DFT-calculated λ_{\max} values of chromophores 9–11. Figures S10–S29: ¹H ¹³C NMR and IR spectra of compounds 6, 9–11.

Author Contributions: Conceptualization, E.V.V., F.B. and S.A.; methodology, Y.A.K., F.B. and S.A.; investigation, E.V.V., P.I.P., A.B. and F.B.; writing—original draft preparation, E.V.V., P.I.P., F.B. and S.A.; writing—review and editing, E.V.V., S.A. and F.B.; supervision, G.L.R.; project administration, V.N.C. All authors have read and agreed to the published version of the manuscript.

Funding: This research was funded by Russian Science Foundation, grant number No. 19-13-00234. F.B. is indebted to the Czech Science Foundation (22-14988S).

Institutional Review Board Statement: Not applicable.

Informed Consent Statement: Not applicable.

Data Availability Statement: The data are available on request from the corresponding authors.

Conflicts of Interest: The authors declare no conflict of interest.

Sample Availability: Samples of the compounds 9–11 are available from the authors.

References

1. Bureš, F. Fundamental aspects of property tuning in push-pull molecules. *RSC Adv.* **2014**, *4*, 58826–58851. [[CrossRef](#)]
2. Beverina, L.; Pagani, G.A. π -Conjugated zwitterions as paradigm of donor-acceptor building blocks in organic-based materials. *Acc. Chem. Res.* **2014**, *47*, 319–329. [[CrossRef](#)] [[PubMed](#)]
3. Kivala, M.; Diederich, F. Acetylene-derived strong organic acceptors for planar and nonplanar push-pull chromophores. *Acc. Chem. Res.* **2009**, *42*, 235–248. [[CrossRef](#)] [[PubMed](#)]
4. Kato, S.; Diederich, F. Non-planar push-pull chromophores. *Chem. Commun.* **2010**, *46*, 1994–2006. [[CrossRef](#)]
5. Meier, H. Conjugated oligomers with terminal donor-acceptor. *Angew. Chem. Int. Ed.* **2005**, *44*, 2482–2506. [[CrossRef](#)]
6. Kivala, M.; Diederich, F. Conjugation and optoelectronic properties of acetylenic scaffolds and charge-transfer chromophores. *Pure Appl. Chem.* **2008**, *80*, 411–427. [[CrossRef](#)]
7. Ipu, M.; Billon, C.; Micouin, G.; Samarut, J.; Andraud, C.; Bretonniere, Y. Fluorescent push-pull responsive probes for ratiometric detection of intracellular pH. *Org. Biomol. Chem.* **2014**, *2*, 3641–3648. [[CrossRef](#)]
8. Lee, S.-C.; Heo, J.; Woo, H.C.; Lee, J.-A.; Seo, Y.H.; Lee, C.-L.; Kim, S.; Kwon, O.-P. Fluorescent molecular rotors for viscosity. *Chem.-Eur. J.* **2018**, *24*, 13706–13718. [[CrossRef](#)]
9. Lee, S.; Kim, S.-H.; Lee, S.; Lee, Y.; Lee, S.; Yang, K.-H.; Wang, K.-K.; Han, W.-S. Pyridazine-carbazole based fluorescent probes for volatile acid detection. *Dyes Pigment.* **2021**, *194*, 109613.
10. Dal Molin, M.; Verolet, Q.; Soleimanpour, S.; Matile, S. Mechanosensitive membrane probes. *Chem.-Eur. J.* **2015**, *21*, 6012–6021. [[CrossRef](#)]
11. Ji, J.M.; Zhou, H.; Kim, H.K. Rational design criterion for D- π -A structured organic and porphyrin sensitizers for highly efficient dyes-sensitized solar cells. *J. Mater. Chem. A* **2018**, *6*, 14518–14545. [[CrossRef](#)]
12. Lu, J.; Liu, S.; Wang, M. Push-pull zinc porphyrins as light-harvesters for efficient dye sensitized solar cells. *Front. Chem.* **2018**, *6*, 541. [[CrossRef](#)] [[PubMed](#)]
13. Yella, A.; Mai, C.-L.; Zakeeruddin, S.M.; Chang, S.N.; Hsieh, C.-H.; Yeh, C.-Y.; Graetzel, M. Molecular engineering of push-pull porphyrin dyes for highly efficient dye-sensitized solar cells: The role of benzene spacers. *Angew. Chem. Int. Ed.* **2014**, *53*, 2973–2977. [[CrossRef](#)]
14. Verbitskiy, E.V.; Rusinov, G.L.; Chupakhin, O.N.; Charushin, V.N. Azines as unconventional anchoring groups for dye-sensitized solar cells: The first decade of research advances and future outlook. *Dyes Pigment.* **2021**, *194*, 109650. [[CrossRef](#)]
15. Li, W.; Ye, L.; Li, S.; Yao, H.; Ade, H.; Hou, J. A high-efficiency organic solar cell enabled by the strong intramolecular electron push-pull effect of the nonfullerene acceptor. *Adv. Mater.* **2018**, *30*, 1707170. [[CrossRef](#)] [[PubMed](#)]
16. Du, S.; Yao, N.; Liu, S.; Xu, Y.; Cao, J.; Zhuang, W.; Yu, J.; Wang, N.; Yu, D.; Zhang, F.; et al. Nonfullerene acceptors from thieno[3,2-*b*]thiophene-fused naphthalene donor with six-member-ring connection for efficient organic solar cells. *Dyes Pigment.* **2021**, *185*, 108892. [[CrossRef](#)]
17. Simón Marqués, P.; Castán, J.M.A.; Raul, B.A.L.; Londi, G.; Ramirez, I.; Pshenichkov, M.S.; Beljonne, D.; Walzer, K.; Blais, M.; Allain, M.; et al. Triphenylamine/tetracyclobutadiene-based π -conjugated push-pull molecules end-capped with arene platforms: Synthesis, photophysics, and photovoltaic response. *Chem.-Eur. J.* **2020**, *26*, 16422–16433. [[CrossRef](#)] [[PubMed](#)]
18. Ostroverkhova, O. Organic Optoelectronic Materials: Mechanisms and Applications. *Chem. Rev.* **2016**, *116*, 13279–13412. [[CrossRef](#)]
19. Payne, A.-J.; Rice, N.A.; McAfee, S.M.; Lo, S.; Josse, P.; Cabanetos, P.; Rishko, C.; Lessard, B.H.; Welch, G.C. Donor or Acceptor? How selection of the rylene imide end cap impacts the polarity of π -conjugated molecules for organic electronics. *ACS Appl. Energy Mater.* **2019**, *1*, 4906–4916. [[CrossRef](#)]

20. Liu, J.; Ouyang, C.; He, W.; Cao, A. Progress in the enhancement of electro-optic coefficients and orientation stability for organic second-order nonlinear optical materials. *Dyes Pigment.* **2020**, *181*, 108509. [[CrossRef](#)]
21. Wong, M.Y.; Zysman-Colman, E. Purely organic thermally activated delayed fluorescence materials for organic light-emitting diodes. *Adv. Mater.* **2017**, *29*, 1605444. [[CrossRef](#)] [[PubMed](#)]
22. Moreno-Yruela, C.; Garín, J.; Orduna, J.; Franco, S.; Quintero, E.; López-Navarrete, J.T.; Diosdado, B.E.; Villacampa, B.; Casado, J.; Andreu, R. D- π -A compounds with tunable intramolecular charge transfer achieved by incorporation of bitenolide nitriles as acceptor moieties. *J. Org. Chem.* **2015**, *80*, 12115–12128. [[CrossRef](#)]
23. Tydlitát, J.; Fecková, M.; Le Poul, P.; Pytela, O.; Klikar, M.; Rodríguez-López, J.; Robin-le Guen, F.; Achelle, S. Influence of donor-substituents on triphenylamine chromophores bearing pyridine fragments. *Eur. J. Org. Chem.* **2019**, *2019*, 1921–1930. [[CrossRef](#)]
24. Klikar, M.; Bureš, F.; Pytela, O.; Mikysek, T.; Padělková, Z.; Barsella, A.; Dorkenoo, K.; Achelle, S. N,N'-Dibutylbarbituric acid as an acceptor moiety in push-pull chromophores. *New J. Chem.* **2013**, *37*, 4230–4240. [[CrossRef](#)]
25. Stefko, M.; Tzirakis, M.D.; Breiten, B.; Ebert, M.O.; Dumele, O.; Schweizer, W.B.; Gisselbrecht, J.P.; Boudon, C.; Beels, M.T.; Biaggio, I.; et al. Donor-acceptor (D-A)-substituted polyynene chromophores: Modulation of their optoelectronic properties by varying the length of the acetylene spacer. *Chem.-Eur. J.* **2013**, *19*, 12693–12704. [[CrossRef](#)]
26. Achelle, S.; Rodríguez-López, J.F.; Robin-Le Guen, F. Photoluminescence properties of Aryl-, Arylvinyl-, and arylethynylpyrimidine derivatives. *ChemistrySelect* **2018**, *3*, 1852–1886. [[CrossRef](#)]
27. Meti, P.; Park, H.-H.; Gong, Y.-D. Recent developments in pyrazine functionalized pi-conjugated materials for optoelectronic applications. *J. Mater. Chem. C* **2020**, *8*, 352–379. [[CrossRef](#)]
28. Nosova, E.V.; Achelle, S.; Lipunova, G.N.; Charushin, V.N.; Chupakhin, O.N. Functionalized benzazines as luminescent materials and component for optoelectronics. *Russ. Chem. Rev.* **2019**, *88*, 1128–1178. [[CrossRef](#)]
29. Verbitskiy, E.V.; Rusinov, G.L.; Chupakhin, O.N.; Charushin, V.N. Design of fluorescent sensors based on azaheterocyclic push-pull systems towards nitroaromatic explosives and related compounds: Review. *Dyes Pigment.* **2020**, *180*, 108141. [[CrossRef](#)]
30. Fecková, M.; Le Poul, P.; Bureš, F.; Robin-le Guen, F.; Achelle, S. Nonlinear optical properties of pyrimidine chromophores. *Dyes Pigment.* **2020**, *182*, 108659. [[CrossRef](#)]
31. Gupta, S.; Milton, M.D. Design and synthesis of novel V-shaped AIEE active quinoxalines for acidochromic applications. *Dyes Pigment.* **2019**, *165*, 474–487. [[CrossRef](#)]
32. Rakitin, O.A.; Zibarev, A.V. Synthesis and Applications of 5-Membered Chalcogen-Nitrogen π -Heterocycles with Three Heteroatoms. *Asian J. Org. Chem.* **2018**, *7*, 2397–2416. [[CrossRef](#)]
33. Konstantinova, L.S.; Rakitin, O.A. Chalcogen exchange in chalcogen–nitrogen π -heterocycles. *Mendeleev Commun.* **2021**, *31*, 433–441. [[CrossRef](#)]
34. Sheremetev, A.B.; Yudin, I.L. Advances in the chemistry of furazano[3,4-*b*]pyrazines and their analogues. *Russ. Chem. Rev.* **2003**, *72*, 87–100. [[CrossRef](#)]
35. Makhova, N.N.; Belen'kii, L.I.; Gazieva, G.A.; Dalinger, I.L.; Konstantinova, L.S.; Kuznetsov, V.V.; Kravchenko, A.N.; Krayushkin, M.M.; Rakitin, O.A.; Starosotnikov, A.M.; et al. Progress in the chemistry of nitrogen-, oxygen- and sulfur-containing heterocyclic systems. *Russ. Chem. Rev.* **2020**, *89*, 55–124. [[CrossRef](#)]
36. Verbitskiy, E.V.; Kvashnin, Y.A.; Baranova, A.A.; Yakovleva, Y.A.; Khokhlov, K.O.; Rusinov, G.L.; Charushin, V.N. 9-Ethyl-3-(6-(het)aryl-[1,2,5]oxadiazolo[3,4-*b*]pyrazin-5-yl)-9H-carbazoles: Synthesis and study of sensitivity to nitroaromatic compounds. *Russ. Chem. Bull.* **2018**, *67*, 1078–1082. [[CrossRef](#)]
37. Verbitskiy, E.V.; Kvashnin, Y.A.; Baranova, A.A.; Khokhlov, K.O.; Chuvashov, R.D.; Yakovleva, Y.A.; Makarova, N.I.; Vetrova, E.V.; Metelitsa, A.V.; Rusinov, G.L.; et al. Novel fluorophores based on imidazopyrazine derivatives: Synthesis and photophysical characterization focusing on solvatochromism and sensitivity towards nitroaromatic compounds. *Dyes Pigment.* **2019**, *168*, 248–256. [[CrossRef](#)]
38. Kvashnin, Y.A.; Verbitskiy, E.V.; Eltsov, O.S.; Slepukhin, P.A.; Tameev, A.R.; Nekrasova, N.V.; Rusinov, G.L.; Nunzi, J.-M.; Chupakhin, O.N.; Charushin, V.N. Dibenzo[*f,h*]furazano[3,4-*b*]quinoxalines: Synthesis by intramolecular cyclization through direct transition metal-free C–H functionalization and electrochemical, photophysical, and charge mobility characterization. *ACS Omega* **2020**, *5*, 8200–8210. [[CrossRef](#)]
39. Verbitskiy, E.V.; Achelle, S.; Bureš, F.; Le Poul, P.; Barsella, A.; Kvashnin, Y.A.; Rusinov, G.L.; Robin-le Guen, F.; Chupakhin, O.N.; Charushin, V.N. Synthesis, photophysical and nonlinear optical properties of [1,2,5]oxadiazolo[3,4-*b*]pyrazine-based linear push-pull systems. *J. Photochem. Photobiol. A Chem.* **2021**, *404*, 112900. [[CrossRef](#)]
40. Kulhánek, J.; Bureš, F.; Opršal, J.; Kuznik, W.; Mikysek, T.; Růžička, A. 1,4-phenylene and 2,5-thiophenylene π -linkers in charge-transfer chromophores. *Asian J. Org. Chem.* **2013**, *2*, 422–431. [[CrossRef](#)]
41. Marco, A.B.; Burrezo, P.M.; Mosteo, L.; Franco, S.; Garín, J.; Orduna, J.; Diosdado, B.E.; Villacampa, B.; Lopez Navarrete, J.T.; Casado, J.; et al. Polarization, second order nonlinear optical properties and electrochromism in 4*H*-pyranilidene chromophores with quinoid/aromatic thiophene ring bridge. *RSC Adv.* **2015**, *5*, 231–242. [[CrossRef](#)]
42. He, J.; Mathew, S.M.; Cornett, S.D.; Grundy, S.C.; Hartley, C.S. Ortho-phenylene oligomers with terminal push-pull substitution. *Org. Biomol. Chem.* **2012**, *10*, 3398–3405. [[CrossRef](#)]
43. Hammer, B.A.G.; Müllen, K. Dimensional evolution of polyphenylenes: Expanding in all directions. *Chem. Rev.* **2016**, *116*, 2103–2140. [[CrossRef](#)] [[PubMed](#)]

44. Reichardt, C. Solvatochromic dyes as solvent polarity indicators. *Chem. Rev.* **1994**, *94*, 2319–2358. [[CrossRef](#)]
45. Lartia, R.; Allain, C.; Bordeau, G.; Schmidt, F.; Fiorini-Desbuischert, C.; Charra, F.; Teulade Fichou, M.-P. Synthetic strategies to derivatizable triphenylamine displaying high two-photon absorption. *J. Org. Chem.* **2008**, *73*, 1732–1744. [[CrossRef](#)]
46. Katan, C.; Charlot, M.; Mongin, O.; Le Droumaguet, C.; Juikov, V.; Terenziani, F.; Badaeva, E.; Tretiak, S.; Blanchard-Desce, M. Simultaneous, control of emission localization and two-photon absorption efficiency in dissymmetrical chromophores. *J. Phys. Chem. B* **2010**, *114*, 3152–3169. [[CrossRef](#)]
47. Merkt, F.K.; Höwedes, S.P.; Gers-Panther, C.F.; Gruber, I.; Jeniak, C.; Müller, T.J.J. Three component activation/alkynylation/cyclocondensation (AACC) synthesis of enhanced emission solvatochromic 3-ethynylquinoxalines. *Chem. Eur. J.* **2018**, *24*, 8114–8125. [[CrossRef](#)]
48. Fecková, M.; Le Poul, P.; Robin-le Guen, F.; Roisnel, T.; Pytela, O.; Klikar, M.; Bureš, F.; Achelle, S. 2,4-Distyryl and 2,4,6-tristyrylpyrimidines: Synthesis and photophysical properties. *J. Org. Chem.* **2018**, *83*, 11712–11726. [[CrossRef](#)]
49. Achelle, S.; Robin-le Guen, F. Emission properties of diazines chromophores: Structure properties relationship. *J. Photochem. Photobiol. A Chem.* **2017**, *348*, 281–286. [[CrossRef](#)]
50. Shen, X.Y.; Yuan, W.Z.; Liu, Y.; Zhao, Q.; Liu, P.; Ma, Y.; Williams, I.D.; Qin, A.; Sun, J.Z.; Tang, B.Z. Fumaronitrile-based fluorogen: Red to near-infrared fluorescence, aggregation-induced emission, solvatochromism, and twisted intramolecular charge transfer. *J. Phys. Chem. C* **2012**, *116*, 10541–10547. [[CrossRef](#)]
51. Gupta, S.; Milton, M.D. Novel Y-shaped AIEE-TICT active π -extended quinoxalines-based donor-acceptor molecules displaying acidofluorochromism and temperature dependent emission. *J. Photochem. Photobiol. A Chem.* **2022**, *424*, 113630. [[CrossRef](#)]
52. Luo, J.; Xie, Z.; Lam, J.W.Y.; Cheng, L.; Chen, H.; Qiu, C.; Kwok, H.S.; Zhan, X.; Liu, Y.; Zhu, D.; et al. Aggregation-induced emission of 1-methyl-1,2,3,4,5-pentaphenylsilole. *Chem. Commun.* **2001**, *18*, 1740–1741. [[CrossRef](#)] [[PubMed](#)]
53. Chen, Y.; Lam, J.W.Y.; Kwok, R.T.K.; Liu, B.; Tang, B.Z. Aggregation-induced emission: Fundamental understanding and future developments. *Mater. Horiz.* **2019**, *6*, 428–433. [[CrossRef](#)]
54. Singer, K.D.; Garito, A.F. Measurements of molecular second order optical susceptibilities using dc induced second harmonic generation. *J. Chem. Phys.* **1981**, *75*, 3572. [[CrossRef](#)]
55. Levine, B.F.; Bethea, C.G. Molecular hyperpolarizabilities determined from conjugated and nonconjugated liquids. *Appl. Phys. Lett.* **1974**, *24*, 445. [[CrossRef](#)]
56. Ledoux, I.; Zyss, J. Influence of the molecular environment in solution measurements of the second order optical susceptibility for urea derivatives. *Chem. Phys.* **1982**, *73*, 203–213. [[CrossRef](#)]
57. Frisch, M.J.; Trucks, G.W.; Schlegel, H.B.; Scuseria, G.E.; Robb, M.A.; Cheeseman, J.R.; Scalmani, G.; Barone, V.; Petersson, G.A.; Nakatsuji, H.; et al. *Gaussian 16, Revision A.03*; Gaussian, Inc.: Wallingford, CT, USA, 2016.
58. Bird, C.W. The application of new aromaticity index to six-membered ring heterocycles. *Tetrahedron* **1986**, *42*, 89–92. [[CrossRef](#)]
59. Bird, C.W. A new aromaticity index and its application to five-membered heterocycles. *Tetrahedron* **1985**, *41*, 1409–1414. [[CrossRef](#)]
60. Kvashnin, Y.A.; Verbitskiy, E.V.; Zhilina, E.F.; Rusinov, G.L.; Chupakhin, O.N.; Charushin, V.N. Synthesis of Heteroannulated Indolopyrazines through Domino N–H Palladium-Catalyzed/Metal-Free Oxidative C–H Bond Activation. *ACS Omega* **2020**, *5*, 15681–15690. [[CrossRef](#)]
61. Taniguchi, M.; Lindsey, J.S. Database of absorption and fluorescence spectroscopy of >300 common compounds for use in photochemical CAD. *Photochem. Photobiol.* **2018**, *94*, 290–327. [[CrossRef](#)]
62. Ulrich, G.; Barsella, A.; Boeglin, A.; Niu, S.; Ziessel, R. BODIPY-bridged push-pull chromophores for nonlinear optical applications. *ChemPhysChem* **2014**, *15*, 2693–2700. [[CrossRef](#)] [[PubMed](#)]